JACS
JOURNAL OF THE AMERICAN CHEMICAL SOCIETY
pubs.acs.org/JACS
Article

Multifaceted View on the Mechanism of a Photochemical Deracemization Reaction

Roger Jan Kutta,[⊥] Johannes Großkopf,[⊥] Nils van Staalduinen, Antonia Seitz, Philipp Pracht, Stefan Breitenlechner, Christoph Bannwarth,* Patrick Nuernberger,* and Thorsten Bach*

Cite This: J. Am. Chem. Soc. 2023, 145, 2354−2363

Read Online

ACCESS | Metrics & More | Article Recommendations | Supporting Information

ABSTRACT: Upon irradiation in the presence of a chiral benzophenone catalyst (5 mol %), a racemic mixture of a given chiral imidazolidine-2,4-dione (hydantoin) can be converted almost quantitatively into the same compound with high enantiomeric excess (80−99% *ee*). The mechanism of this photochemical deracemization reaction was elucidated by a suite of mechanistic experiments. It was corroborated by nuclear magnetic resonance titration that the catalyst binds the two enantiomers by two-point hydrogen bonding. In one of the diastereomeric complexes, the hydrogen atom at the stereogenic carbon atom is ideally positioned for hydrogen atom transfer (HAT) to the photoexcited benzophenone. Detection of the protonated ketyl radical by transient absorption revealed hydrogen abstraction to occur from only one but not from the other hydantoin enantiomer. Quantum chemical calculations allowed us to visualize the HAT within this complex and, more importantly, showed that the back HAT does not occur to the carbon atom of the hydantoin radical but to its oxygen atom. The achiral enol formed in this process could be directly monitored by its characteristic transient absorption signal at $\lambda \cong 330$ nm. Subsequent tautomerization leads to both hydantoin enantiomers, but only one of them returns to the catalytic cycle, thus leading to an enrichment of the other enantiomer. The data are fully consistent with deuterium labeling experiments and deliver a detailed picture of a synthetically useful photochemical deracemization reaction.

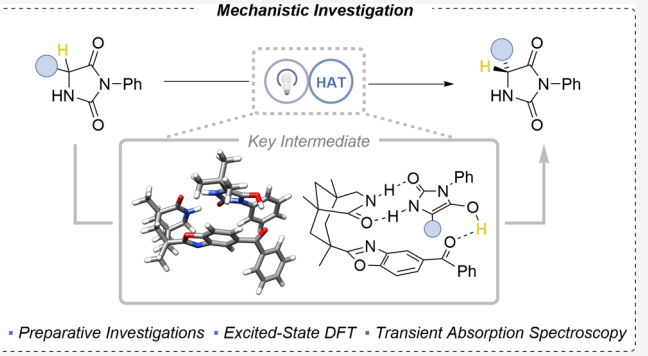

INTRODUCTION

Enantiomerically pure compounds, i.e., chiral compounds sold as single enantiomers, represent a huge class of chemicals with sales exceeding 100 billion US-$ per year.[1] The market for enantiomerically pure drugs displays even higher sales figures.[2] Although research in enantioselective (asymmetric) catalysis has led to remarkably efficient processes for the syntheses of chiral compounds,[3] it is frequently less expensive and more efficient to prepare chiral compounds as a racemic mixture and to separate the enantiomers subsequently.[4] The latter approach is particularly appealing if both enantiomers of a chiral compound are required. If this is not the case, e.g., in many pharmaceutical applications, the unwanted enantiomer is a waste product, and it is desirable to find ways of proper recycling or to generate enantiomerically pure compounds from their racemates. In the latter context, deracemization reactions have received considerable attention,[5] and most methods to perform deracemization have until recently relied on the stoichiometric conversion of the respective racemate into an achiral intermediate, which is subsequently or in situ converted by a chiral reagent to the desired enantiomer. A key requirement for a deracemization reaction is the existence of two distinct steps which are not simply the reversal of each other. In an equilibrium situation, the racemate is entropically favored, and this preference cannot be overcome in a closed catalytic system violating the principle of microscopic reversibility.[6] Based on pioneering efforts in the 1960s and 1970s,[7] photochemical deracemization reactions have been studied more closely in the last five years.[8] The key idea is to decouple a thermal reaction step from a photochemical event, enabling the enrichment of a single enantiomer (Scheme 1). Two different approaches may be considered: (1) A chiral photocatalyst can be used to differentiate between the two substrate enantiomers and to form an achiral intermediate from which the respective substrate is formed thermally in an unselective fashion. If this cycle is continuously repeated, the enantiomer that is not or only slowly processed in the photochemical step will be enriched. (2) Alternatively, the photochemical step can occur unselectively, and a chiral

Received: October 24, 2022
Published: January 20, 2023

https://doi.org/10.1021/jacs.2c11265
J. Am. Chem. Soc. 2023, 145, 2354−2363

Scheme 1. Photochemical Deracemization by a Chiral Catalyst: Enrichment of a Single Enantiomer Is Possible by Selective Excitation or by a Selective Reaction of the Intermediate

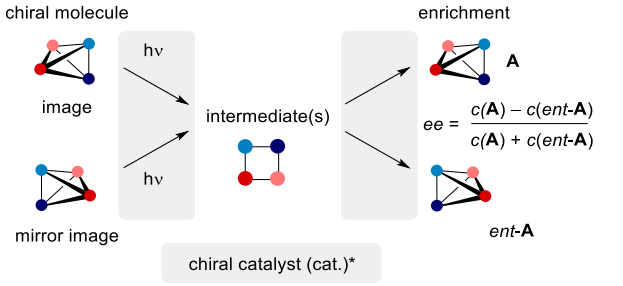

catalyst can be used to form one of the substrate enantiomers in an enantioselective fashion. In the latter scenario, it is desirable that the thermal step is compatible with the photochemical step.[9] If not, the reaction might be preferably performed in two separate steps and bears the characteristics of an enantioselective catalytic reaction but not of a deracemization.[10]

In 2018, our group reported the first photochemical deracemization reaction that delivered chiral organic compounds in high yields and enantioselectivities.[11] Chiral allene lactams were successfully employed as substrates, and a chiral triplet sensitizer (2.5 mol %) was utilized to differentiate between the two substrate enantiomers (17 examples, 52−99% yield, 89−97% *ee*). Achiral diradical **IN1** was postulated as a triplet intermediate based on analogy to known allene triplets,[12] corroborated by subsequent calculations on the deracemization of chiral 2,3-butadienamides.[13] Since then, we have studied several reactions in which achiral intermediates **IN** are selectively formed from a chiral precursor by triplet sensitization according to approach (1) mentioned above (Figure 1). Putative triplet intermediates include diradicals **IN2** (sulfoxide deracemization),[14] **IN3** (cyclopropane deracemization),[15] and **IN4** (alkene deracemization).[16] Knowles, Miller, and co-workers reported in 2019 a dual catalysis approach, in which radical intermediates like **IN5** were formed by a selective photocatalytic reaction and further converted to the cyclic urea substrates by a second enantioselective step on the ground state (15 examples, 90−99% yield, 62−92% *ee*).[17] A chiral phosphoric acid (5 mol %) was employed to allow for differentiation in the first step (radical formation) and a chiral thiol (5 mol %) for the selective hydrogen atom transfer (HAT).

More recently, Meggers and co-workers reported on the formation of chiral enolate intermediates in an unselective photochemical step which were subsequently protonated diastereoselectively via chiral-at-metal rhodium (*[Rh]) enolate **IN6**.[18] In a related approach, taken by Luo and co-workers,[19] a chiral amine was used as the catalyst to promote an enantioselective protonation of (*Z*)-enamine **IN7** which was diastereoselectively generated by triplet-sensitized *E*/*Z*-isomerization.[20] Also in this case, the protonation step is responsible for the preferential formation of a major enantiomer. So far, only the 1,3-diradical **IN3** was observed by transient absorption spectroscopy,[15b] whereas all other intermediates **IN** were postulated and their immediate detection has not been reported.

While all our previous work had focused on the generation of achiral intermediates by triplet sensitization,[11,13−16] we have recently started to investigate different modes of action by which chiral substrates would be differentiated in a photochemical step. In a first study, benzophenone (+)-**2** was found to deliver high enantioselectivities in the photochemical deracemization of hydantoins *rac*-**1** (Scheme 2).[21] A high

Scheme 2. Photochemical Deracemization of Hydantoins *rac*-1 Catalyzed by Chiral Benzophenone (+)-2

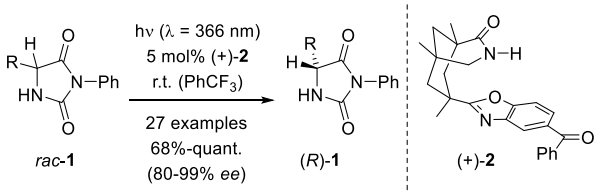

preference for the respective (*R*)-enantiomers (*R*)-**1** was recorded, and circumstantial evidence was collected, which suggested that photoexcited benzophenone (+)-**2** enables a selective HAT[22] from one of the two hydantoins.

Although the first step of the reaction appeared intuitive, the further fate of the intermediate remained unclear. In particular, the thermal pathway which leads to the formation of the hydantoin after HAT required further studies. We have now undertaken a suite of mechanistic experiments to shed light on the course of the deracemization reaction. Based on quantum chemical calculations and supported by the spectroscopic detection of intermediates, a clear picture of the reaction pathway has evolved which we present in this manuscript.

RESULTS AND DISCUSSION

Side Reactions, Association Constants, and Labeling Experiments. For reasons of compound supply, most studies of this section and all transient absorption experiments (vide infra) were performed with benzophenone (−)-**2** (Figure 2).

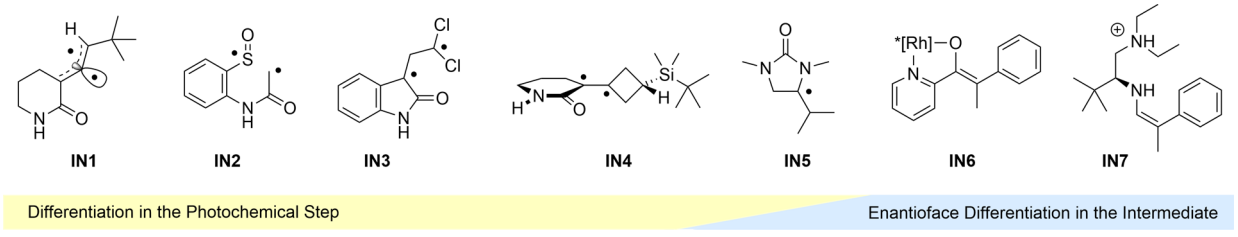

Figure 1. Typical intermediates **IN1**−**IN7** invoked in photochemical deracemization reactions: Intermediates **IN1**−**IN4** are generated predominantly from one substrate enantiomer while intermediates **IN6** and **IN7** react enantioselectively. For intermediate **IN5**, both modes of action operate (two chiral catalysts).

https://doi.org/10.1021/jacs.2c11265
J. Am. Chem. Soc. 2023, 145, 2354−2363

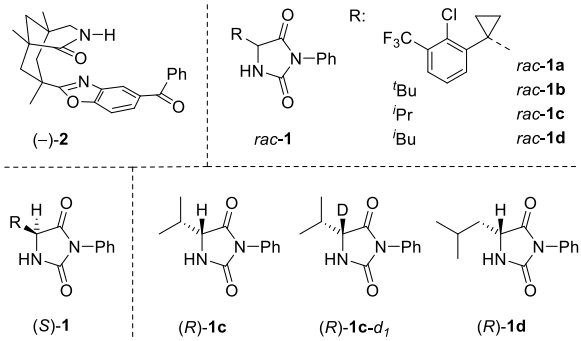

Figure 2. Structure of the chiral catalyst (−)-**2** and of hydantoins *rac*-**1** used in this study. The use of catalyst (−)-**2** leads to the preferred formation of (*S*)-configured hydantoins (*S*)-**1** in the deracemization reaction. Enantiomerically pure (*R*)-hydantoins were used for kinetic experiments.

Expectedly, the catalyst favors in the photochemical reaction the opposite enantiomers compared to benzophenone (+)-**2**, i.e., not the (*R*)-hydantoins but the respective (*S*)-enantiomers are formed. This was verified by performing the deracemization of hydantoin *rac*-**1a** as a control experiment. In previous work, we had isolated the enantiomer (*R*)-**1a** with (+)-**2** as the catalyst in 87% yield and with 94% *ee*.[21] When the same reaction was conducted under identical conditions with catalyst (−)-**2**, the (*S*)-enantiomer (*S*)-**1a** was isolated in 86% yield and with 94% *ee*.

The use of compound *rac*-**1a** or its enantiomers for several of the mechanistic investigations was due to its high solubility in trifluorotoluene which is the preferred solvent for the deracemization experiments. To simplify the nature of the substituent R, the *tert*-butyl-substituted hydantoin **1b** was the preferred model compound for the computational studies (vide infra). Further mechanistic experiments were performed with the valine- and leucine-derived hydantoins **1c** and **1d**.

A key feature of the deracemization experiments performed with benzophenone **2** relies on its propensity for hydrogen abstraction[23] in the excited triplet $n\pi^*$ state.[24] A prerequisite for the HAT to be selective is the formation of the respective 1:1 complex with the individual enantiomers. We therefore studied these complexes by nuclear magnetic resonance (NMR) titration in benzene-d_6 at ambient temperature (20 °C).[25] Indeed, it was confirmed that both enantiomers of hydantoin **1a**, (*R*)-**1a** and (*S*)-**1a**, undergo association to (−)-**2** via two hydrogen bonds (for details see the Supporting Information). The binding constants are not identical, reflecting the fact that the formation of (−)-**2** · (*S*)-**1a** is hampered by Pauli repulsion of the bulky hydantoin substituent and the benzoyl group of the catalyst. Formation of (−)-**2** · (*R*)-**1a** is preferred for steric reasons. Within this complex, the hydrogen atom at the stereogenic center (indicated in bold in Figure 3) is close to the carbonyl group of the benzophenone. In complex (−)-**2** · (*S*)-**1a**, an intramolecular HAT at the stereogenic center has too high a barrier to become kinetically relevant.

Hydrogen abstraction by catalyst (−)-**2** was monitored in kinetic experiments with deuterated and nondeuterated hydantoins. Since the reaction of enantiopure (*R*)-enantiomers leads to a complete inversion of the stereogenic center, the reaction can be followed kinetically by recording the enantiomeric purity over time. In separate experiments, the kinetics were monitored for the reaction of (*R*)-**1** → (*S*)-**1** and

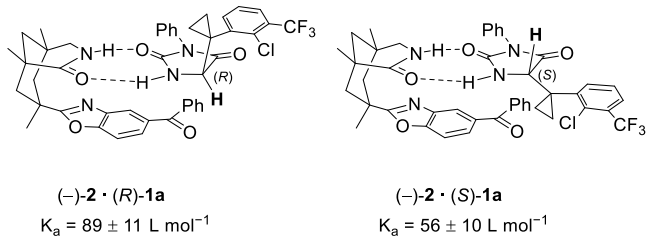

Figure 3. Complexes of chiral benzophenone (−)-**2** with the two enantiomers of hydantoin **1a**: The preferably formed enantiomer (*S*)-**1a** displays a smaller binding constant than its antipode (*R*)-**1a**. Rotation around single bonds is possible at the benzoxazole core, and the conformation is depicted, in which the complex of (−)-**2** and substrates (*R*)-**1** has been found to be the most stable (vide infra).

for (*R*)-**1**-d_1→ (*S*)-**1**-d_1. The rate of conversion was linear within the first 10 min and a kinetic isotope effect k_H/k_D = 1.4 was determined (see the Supporting Information for details). In an intermolecular competition experiment, the inversion of compounds (*R*)-**1** and (*R*)-**1**-d_1 was studied. The observed value was not significantly higher (k_H/k_D = 1.8), which, at first sight, suggested that the HAT has little influence on the rate and selectivity.[26] However, the computational results revealed an equally low kinetic isotope effect (vide infra) which potentially indicates that the HAT step is turnover limiting.

Previous work with deuterated hydantoins had revealed that H/D cross-over occurs during deracemization employing catalyst (+)-**2**.[21] With an equimolar mixture of deuterated, leucine-derived hydantoin **1d**-d_1 and non-deuterated valine-derived hydantoin **1c**, the products also displayed non-deuterated **1d** and deuterated **1c**-d_1 in varying amounts. If a complete inversion was performed, e.g., by going from (*S*)-**1** to (*R*)-**1**, a ca. 50% H/D cross-over was noted. If the starting materials were racemic, the cross-over was ca. 25%, and if the starting material already possessed the correct configuration, there was no cross-over. If one assumes that the deracemization occurs via the protonated (or deuterated) ketyl radical (−)-**3** (Figure 4), the results appeared to suggest that the re-

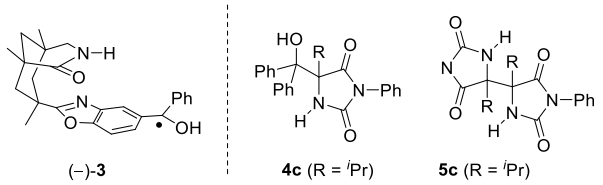

Figure 4. Structure of putative intermediate (−)-**3** and reaction products **4c** and **5c** obtained upon irradiation of a sample containing parent benzophenone (BP) and the valine-derived hydantoin **1c** (2 equiv, λ = 350 nm, $PhCF_3$).

delivery of the hydrogen or deuterium atom occurs not always to the same molecule it had been abstracted from. Radical-radical coupling products were not detected, however. In contrast, when using parent benzophenone (PhCOPh, BP) to induce a racemization reaction in valine-derived hydantoin (*S*)-**1c**, significant amounts of coupling products **4c** and **5c** were observed.

Product **4c** is the 1:1 adduct of the protonated ketyl radical with the hydantoin radical formed by hydrogen abstraction. Product **5c** (isolated as a single diastereoisomer) is the product of a radical-radical combination between two hydantoin radicals. The results indicate that upon leaving the solvent

https://doi.org/10.1021/jacs.2c11265
J. Am. Chem. Soc. 2023, 145, 2354−2363

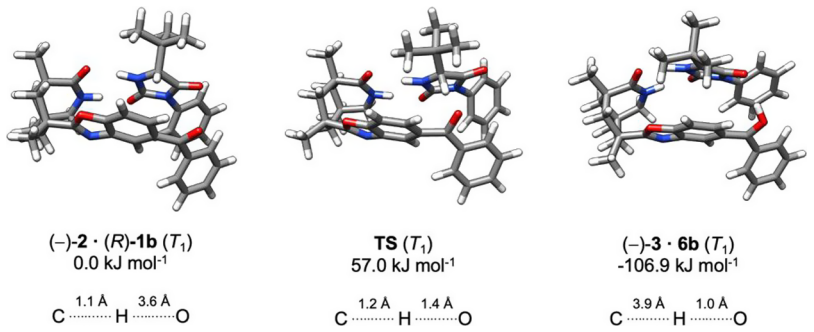

Figure 5. Calculated T_1 structures for (−)-**2** · (*R*)-**1b**, **TS**, and (−)-**3** · **6b** in the deracemization reaction of *rac*-**1b**. Free energies of the corresponding species are calculated relative to (−)-**2** · (*R*)-**1b** at the ωB97X-V/def2-QZVP//PBEh-3c level of theory (see the Supporting Information for details).[29,27] The hydrogen atom of hydantoin is transferred to the catalyst yielding a complex of the protonated ketyl radical (−)-**3** and the hydantoin radical **6b**.

cage, the radicals formed via hydrogen abstraction by photoexcited benzophenone may undergo free radical-radical recombination. To shed light on this issue, we investigated the reaction pathway leading to deracemization of compound *rac*-**1b** by quantum chemical calculations.

Quantum Chemical Calculations on the Hydrogen Atom Transfer. Based on the experimental analyses (NMR and kinetic studies, vide supra), we restricted the computational analysis to the configuration inversion of (*R*)-**1b** assisted by catalyst (−)-**2**. As starting geometry for the HAT in complex (−)-**2** · (*R*)-**1b**, we initially used the previously determined complex structure[21] from a conformational analysis that exhibited the shortest hydrogen−oxygen distance. However, we identified in this work a second, lower energetic conformation by conformational sampling of (−)-**2** · (*R*)-**1b**. Here, the benzoxazole core has undergone a rotation around the single bond to the azabicyclo[3.3.1]nonan-2-one backbone. In the following, we discuss exclusively the results for the energetically more stable conformer (called **min2** in the SI) but provide results for the other conformer (**min1**) in the Supporting Information. The final geometries on the triplet (T_1) state for (−)-**2** · (*R*)-**1b** and the identified HAT intermediate, (−)-**3** · **6b**, were obtained by structure optimization at the PBEh-3c level, which is a low-cost DFT composite method.[27] Intermediate **6b** is the hydantoin radical obtained by HAT from **1b**. The transition state for the HAT was determined by a nudged elastic band optimization with subsequent transition state (TS) optimization on the T_1 state employing the GFN2-xTB method.[28] The identified structure was then re-optimized also at the PBEh-3c level. Details for the optimization procedure can be found in the Supporting Information. The obtained T_1 species involved in the forward HAT are shown in Figure 5.

During the HAT, the proximal hydrogen atom of hydantoin (*R*)-**1b** is transferred to the catalyst, leading to the protonated ketyl radical (−)-**3** and the hydantoin radical **6b**. The distance of the involved hydrogen atom to the carbonyl oxygen atom of the catalyst decreases from 3.6 to 1.0 Å during the HAT. Simultaneously, the distance of the hydrogen atom to the hydantoin carbon increases from 1.1 to 3.9 Å at the chosen level of theory. At the transition state, the hydrogen atom is almost located halfway between the carbon atom (1.2 Å) and the oxygen atom (1.4 Å). Moreover, the initially chiral, tetrahedral carbon atom of (*R*)-**1b** planarizes as the hybridization changes from sp^3 to sp^2, leading to the achiral radical intermediate **6b**.

The low barrier of 57.0 kJ mol^{-1} (ωB97X-V/def2-QZVP//PBEh-3c level[27,29]) found for the HAT confirms the experimentally observed rapid hydrogen transfer to occur at the T_1 state after photoexcitation and intersystem crossing (ISC). At the T_1 surface, the HAT toward (−)-**3** · **6b** is exergonic by −106.9 kJ mol^{-1} relative to (−)-**2** · (*R*)-**1b**. Experimentally, a kinetic isotope effect k_H/k_D = 1.4−1.8 was observed. To compute the theoretical kinetic isotope effect for the aforementioned HAT reaction, the nuclear thermal corrections[29a] to (−)-**2** · (*R*)-**1b** and **TS** were recalculated after changing the mass of the hydrogen involved in the HAT to 2.00141 u (see the Supporting Information for more details). For deuterium, the calculated HAT reaction barrier increases from 57.0 to 58.6 kJ mol^{-1}. This results in a theoretical kinetic isotope effect of 1.9 in good agreement with the experimental value (vide supra). It should be noted that for the higher lying conformer (**min1**, see SI), a lower barrier of 40.6 kJ mol^{-1} was found, which, however, would result in a kinetic isotope effect around 4.7. Hence, based on the fact that conformer **min2** is more stable and reproduces the experimental kinetic isotope effect, we conclude that the photocatalyzed deracemization proceeds via the **min2** conformer and no rotation to the **min1** conformer occurs during the lifetime of the triplet state.

Given that (−)-**3** · **6b** is significantly lower in free energy on the triplet hypersurface than (−)-**2** · (*R*)-**1b**, the back HAT mechanism is expected to proceed in the singlet manifold after reverse ISC has taken place. The reaction is, hence, expected to involve a conical intersection between the open shell and closed shell (S_0) singlet state. The preceding ISC from T_1 to the open shell singlet is readily feasible, since for (−)-**3** · **6b**, the two states are found to be isoenergetic [−106.9 kJ mol^{-1} relative to (−)-**2** · (*R*)-**1b**] and structurally indistinguishable. The energetically lowest S_0/S_1 minimum energy conical intersection (MECI) could be identified by a recently developed sampling algorithm[30] (see the Supporting Information for details). Remarkably, among all sampled structures, no precursor geometry could be identified that would correspond to a *direct* HAT to the prostereogenic carbon atom of radical intermediate **6b**. In conclusion, a back HAT directly forming the hydantoin **1b** can be ruled out. However, the lowest-lying complex structure in the ensemble shows a hydrogen bond between the hydrogen atom of the catalyst and the carbonyl oxygen atom of **6b**. It was found that the identified MECI structure is structurally very similar to another, lower-lying

https://doi.org/10.1021/jacs.2c11265
J. Am. Chem. Soc. 2023, 145, 2354−2363

minimum existing both on the open shell singlet and T_1 surface (Figure 6).

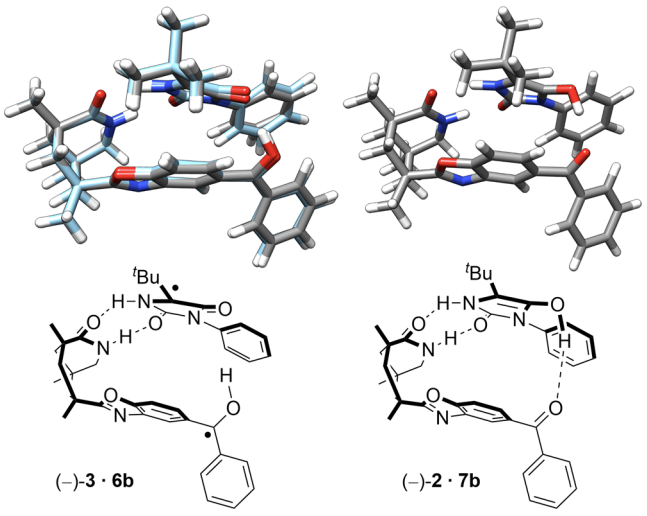

Figure 6. Left: MECI structure optimized at the FOMO-*hh*TDA-BHLYP-D3(BJ)/def2-SV(P) level of theory[31] (gray) and the proximate minimum structure (−)-**3** · **6b** in the open shell singlet (light-blue) optimized at the PBEh-3c[27] level of theory. Right: Ground state (S_0) structure (−)-**2** · **7b** after the back HAT optimized at the PBEh-3c[27] level of theory.

The computed association free energy between (−)-**3** and **6b** was found to be −38.8 kJ mol^{-1}, rendering the complex more stable than (−)-**2** · (*R*)-**1b** (see the Supporting Information for details). The dissociation into free radicals and coupling reactions as observed for BP (vide supra) are therefore avoided. Taken together with the fact that triplet and open shell singlet minima are isoenergetic for (−)-**3** · **6b**, ISC is expected to be easily feasible at this geometry. Once arrived at the singlet manifold, the reaction proceeds nearly barrierless through the MECI (see the Supporting Information). The final minimum structure after the back HAT on the singlet manifold was obtained by PBEh-3c optimizations[27] on the S_0 surface, leading to the noncovalent complex (−)-**2** · **7b** (Figure 6). Compound **7b** is the (achiral) enol[32] tautomer of hydantoin **1b**. The overall pathway for the deracemization process is comprehensively summarized in Figure 7.

The calculation delivered a fully coherent explanation for the abovementioned dichotomy regarding the deuterium scrambling and the side reactions observed with an achiral catalyst (Figure 4). Since the enol form **7** of the hydantoin is the intermediate via which the racemization occurs, scrambling does not occur in any of the intermolecular HAT processes but in the subsequent tautomerization step. The exchange of protons likely occurs in a bimolecular fashion[33] and is thus responsible for the observed H/D scrambling. From a stereochemical perspective, intermediate **7** will tautomerize to both enantiomers (*S*)-**1** and (*R*)-**1** with no preference for any of the two enantiomers. Enantiomer (*R*)-**1** is further processed in a catalytic cycle when bound to sensitizer (−)-**2** and will lead again via radical **6** to the respective enol **7** (Scheme 3). Enantiomer (*S*)-**1** is enriched because it does not display a suitable hydrogen atom for HAT and is found as the prevailing enantiomer if catalyst (−)-**2** is employed.

The introduction has already alluded to the fact that very few intermediates in deracemization reactions have been detected. With the mechanistic scheme outlined above already providing a plausible picture, we felt it crucial to experimentally identify the postulated intermediates by transient absorption spectroscopy. A key issue to be resolved related to the hypothesis that enantiomer (*S*)-**1** was not processed by benzophenone (−)-**2**. If detection of the protonated ketyl radical (−)-**3** was feasible, this question could be reliably answered.

Transient Absorption Spectroscopy. As benzophenone (PhCOPh; BP) is well known to undergo ISC to almost 100% on a ps time scale,[34] ISC will potentially outcompete a potential HAT and, therefore, the excited singlet S_1 of BP may not be relevant for a potential HAT. Accordingly, we focused

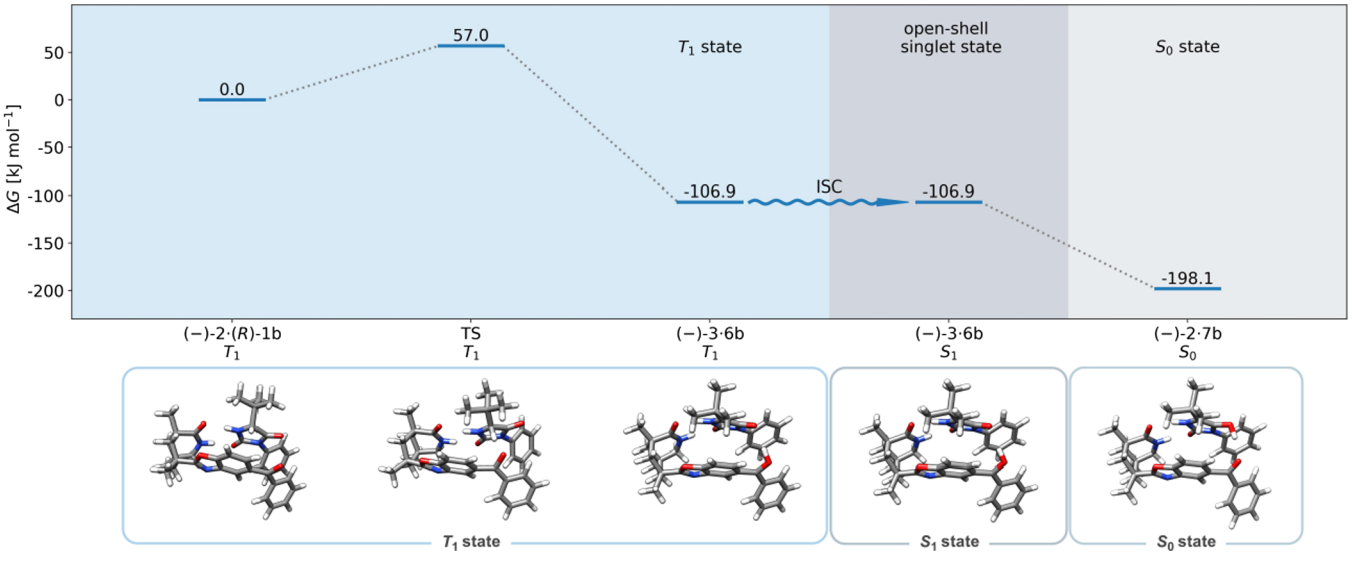

Figure 7. Computed free energy reaction profile for the photocatalytic deracemization of *rac*-**1b**. Electronic energies are calculated at the ωB97X-V/def2-QZVP//PBEh-3c[27,29] level of theory (see the Supporting Information for details on the thermal and solvation contributions). Relative energies are referenced to the free energy of (−)-**2** · (*R*)-**1b** in the T_1 state. A possible ISC step is indicated. Alternatively, triplet recombination is possible, which affords the diradical singlet complex as an intermediate.

https://doi.org/10.1021/jacs.2c11265
J. Am. Chem. Soc. 2023, 145, 2354−2363

Scheme 3. Mechanistic Scheme for the Photochemical Deracemization of Hydantoins *rac*-1 Catalyzed by Chiral Benzophenone (−)-2

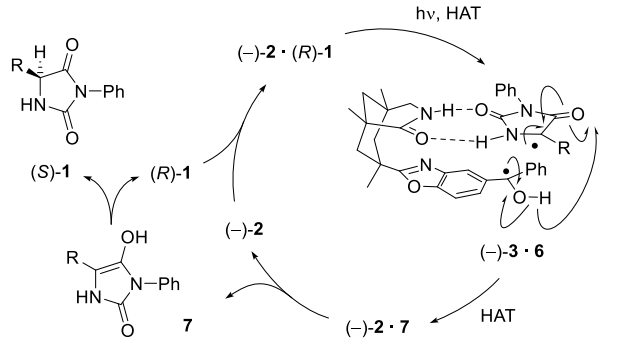

in this study on the triplet (T_1) and subsequent dynamics of the BP moiety on a ns to μs time scale. For acquiring reference spectra of the T_1 as well as the protonated ketyl radical, we initially recorded the transient absorption of BP in $PhCF_3$ and in a $PhCF_3$/cyclohexane (1.65 mM/8.17 M) mixture after excitation at 355 nm. Under the latter conditions, the radical formation should be observed after HAT from the aliphatic cyclohexane to BP.[24] In nondegassed $PhCF_3$, the well-known T_1 spectrum with its characteristic spectrum of two narrow absorption bands peaking at 321 and 525 nm and a shoulder at ca. 450 nm is observed within the duration of the excitation pulse, and decays monoexponentially with a lifetime of 240 ns obeying the pseudo-first order kinetics of diffusion-controlled quenching via energy transfer to molecular oxygen (Figure 8). With an abundance of an aliphatic molecule in the surrounding solvent layer, HAT from cyclohexane to the BP T_1 is observed, as evidenced by a tremendous T_1 lifetime reduction down to ca. 140 ns accompanied by the formation of a new species spectrum ascribed to the protonated BP ketyl radical (^{2}BP-H),[24,35] whose species-associated spectrum (SAS) is given in red in Figure 8d. From spectral (Figure 8d) and temporal (Figure 8f) decomposition of the data, an almost complete forward and back HAT for this system may be found (see the Supporting Information for a more detailed discussion on the analysis). As HAT occurs in the triplet spin system, the triplet-born spin-correlated radical pair will be spin-forbidden for back HAT. Accordingly, it is tempting to speculate that for cyclohexane the rate-limiting factor will be back ISC prior to back HAT (vide infra).

In the case of (−)-**2** in $PhCF_3$, the photophysical properties are totally dictated by the benzophenone moiety, as already seen by a very similar ground state $S_1 \leftarrow S_0$ transition with extinction coefficients in the range of 130 M^{-1} cm^{-1} (Supporting Information and Figure 9). Accordingly, after exciting at 355 nm, (−)-**2** also shows very efficient triplet formation to ^{3}(−)-**2**, which subsequently decays with a lifetime of 206 ns in nondegassed solution (Figure 9a,d,g). As the substrate *rac*-**1a** itself absorbs at 355 nm, we separately recorded its transient absorption. It turned out that besides pump−pulse scatter at 355 nm, the fluorescence of *rac*-**1a** between 400 and 550 nm with a lifetime shorter than the instrumental response as well as a very small−barely detectable−broad absorption band with a lifetime of 470 ns is observed (Figure S8.1). Since this absorption signal is significantly smaller than the strong triplet absorption of ^{3}(−)-**2**, it can be neglected in the transient absorption data obtained from (−)-**2** in the presence of either (*R*)-**1a** or (*S*)-**1a**.

While the presence of (*S*)-**1a** (40 mM) does not result in any changes of the ^{3}(−)-**2** dynamics (Figure 9c,f,i), new spectral contributions in the transient data become evident in the presence of (*R*)-**1a** (40 mM) (Figure 9b). The initial

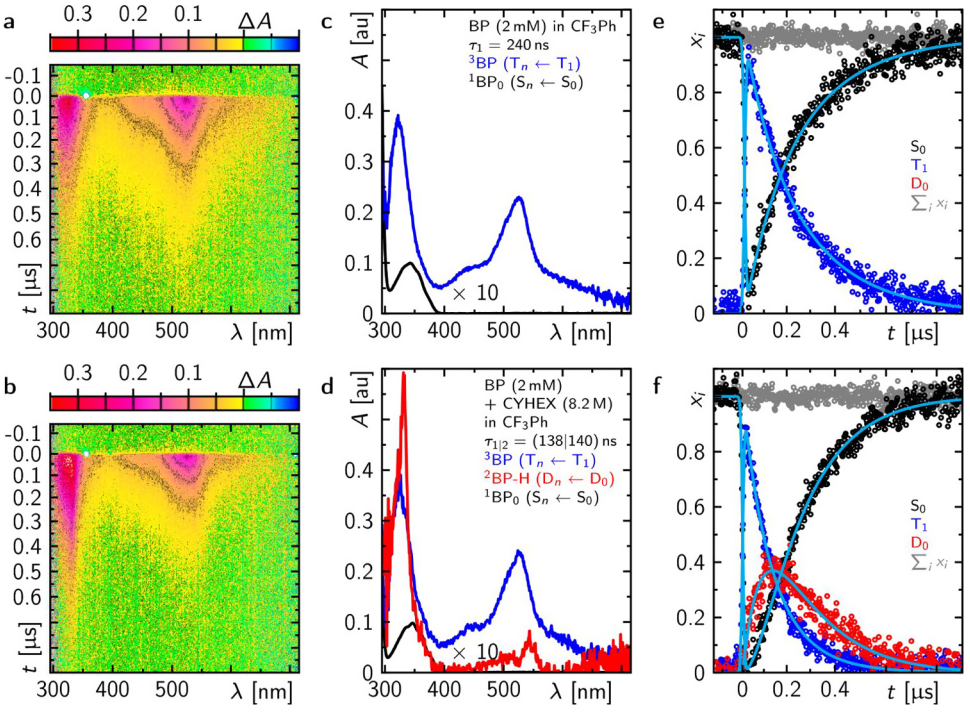

Figure 8. Transient absorption data of benzophenone (BP) in $PhCF_3$ (panels a,c,e) and in $PhCF_3$/cyclohexane (1.65 mM/8.2 M) mixture (panels b,d,f) after excitation at 355 nm. Panels a,b: Time-resolved spectra in false color representation. Panels c−f: Species-associated spectra (panels c,d) and the corresponding mole-fraction over time (together with the global fit shown in cyan) (panels e,f) that contribute to the data in panels a,b.

https://doi.org/10.1021/jacs.2c11265
J. Am. Chem. Soc. 2023, 145, 2354−2363

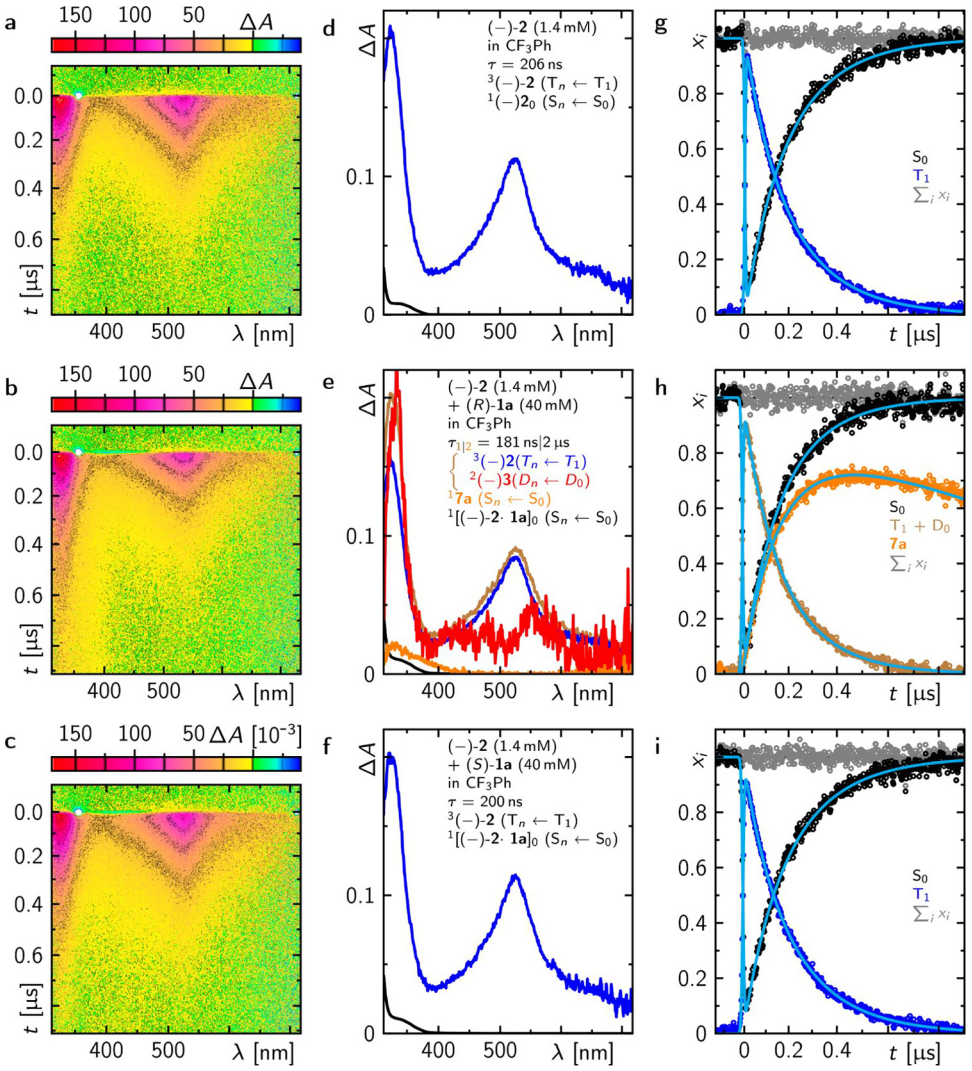

Figure 9. Transient absorption data of (−)-**2** in $PhCF_3$ (panels a,d,g) and in the presence of 40 mM concentration of either (*R*)-**1a** (panels b,e,h) or (*S*)-**1a** (panels c,f,i) after excitation at 355 nm. Panels a−c: Time-resolved spectra in false color representation. Panels d−i: Species-associated spectra (panels d−f) and the corresponding mole-fraction over time (together with the global fit shown in cyan; panels g−i) that contribute to the data in panels a−c. Note that $\sum_i x_i$ in panel h only includes contributions from ^{3}(−)-**2**, ^{2}(−)-**3**, and ^{1}(−)-**2**. In panel e, the spectra of the triplet as well as of the ketyl radical are shown, which were obtained by subtracting 75% of the triplet spectrum (blue spectrum in panels d,f) from the spectrum at t = 0 (sum of all DADS) and corresponding rescaling of the ketyl spectrum by (1−0.75).

transient spectrum formed within the excitation pulse shows in addition to the SAS of ^{3}(−)-**2** further spectral contributions, and all spectral characteristics simultaneously decay with a slightly shorter lifetime of 181 ns compared to the pure ^{3}(−)-**2** decay (compare brown and blue lines in Figure 9e). Subtraction of the ^{3}(−)-**2** contribution (blue line) from this spectrum reveals the SAS of the protonated ketyl radical (−)-**3** as an intermediate (compare red lines in Figures 8d and 9e). The fact that only small signatures of (−)-**3** are observable and that only one lifetime can be determined indicates that the rather efficient radical pair formation after HAT from (*R*)-**1a** to ^{3}(−)-**3** with an overall estimated yield of Φ_{HAT} = 1−181 ns/206 ns = 12% is followed by a faster back HAT so that no substantial concentration of the radical pair is detected.

Considering the concentration of (*R*)-**1a** as [(*R*)-**1a**] = 40 mM, the bimolecular rate constant for forward HAT may be estimated to $k_{HAT} = [(R)\text{-}\mathbf{1a}]^{-1}((181\ \text{ns})^{-1} - (206\ \text{ns})^{-1}) = 1.68 \times 10^7\ M^{-1}\ s^{-1}$. Comparison to the expected fully diffusion-controlled bimolecular rate constant in the order of $10^{10}\ M^{-1}\ s^{-1}$ demonstrates that a very specific diffusive encounter configuration is required for a successful HAT. The spectral features of the counter radical **6** (Scheme 3) are not observed, likely due to significantly lower extinction coefficients, as expected from quantum chemical calculations (compare panels a and b in Figure S8.3). Furthermore, as the back HAT is accompanied by a rise of a new absorption spectrum peaking at ca. 330 nm (orange line in Figure 9), the hydrogen atom is *not* transferred to the initially stereogenic carbon from where it originated. From quantum chemical calculations, it becomes evident that, on the one hand, the initially spin-correlated triplet-born radical pair ^{3}[(−)-**3** · **6a**] first needs to undergo ISC to the singlet radical pair ^{1}[(−)-**3** · **6a**] prior to back HAT and that subsequent back HAT occurs rather to the substrate's carbonyl group, leading to the formation of the enol form **7a** of the initial substrate **1a** and (−)-**2** (see Supporting Video on the molecular dynamics starting from the triplet-born radical pair and Figure S8.3 for comparing the experimental product spectrum with theoretical

https://doi.org/10.1021/jacs.2c11265
J. Am. Chem. Soc. 2023, 145, 2354−2363

spectra of putative **1a**-based intermediates and the corresponding discussion). On a μs timescale, keto-enol tautomerization[33] of enol **7a** will eventually reform (*S*)-**1a** and (*R*)-**1a** in equal amounts. Thus, the feasibility of the deracemization process via the matching combination of the chiral catalyst and substrate is directly reflected in the transient absorption data.

CONCLUSIONS

In summary, a conclusive mechanistic picture has evolved for the photochemical deracemization of hydantoins *rac*-**1**. The reaction is initiated by HAT from the hydantoin to photoexcited benzophenone-based catalyst (−)-**2** or its enantiomer (+)-**2**. Transient absorption spectroscopy revealed unequivocally that HAT occurs only for one but not for the other enantiomer of *rac*-**1**. In the current study, using (−)-**2**, only the (*R*)-enantiomer (*R*)-**1** was processed. Quantum chemical calculations support the hypothesis that the abstracted hydrogen atom of (*R*)-**1** is the hydrogen atom at the stereogenic center, and the calculations delivered a coherent picture of the HAT within the hydrogen-bonded complex between (−)-**2** and (*R*)-**1**. Remarkably, the resulting radicals, protonated ketyl radical (−)-**3** and hydantoin-derived radical **6**, do not dissociate but retain their association via hydrogen bonds. Radical−radical side reactions, as observed for achiral benzophenone in the HAT with hydantoins, are consequently avoided. Instead, a clean back HAT is initiated, which occurs on the singlet hypersurface and which is not the reverse of the forward reaction that had occurred on the triplet hypersurface. Back HAT leads not immediately to the hydantoin but rather to their achiral enol **7**, which subsequently tautomerizes unselectively to either enantiomer (*R*)-**1** or (*S*)-**1**. Since the latter enantiomer is not processed, it is enriched and eventually obtained with high enantioselectivity. In cases where the enantioselectivity is low, the decomposition of the catalyst is likely responsible, inhibiting further conversion of (*R*)-**1**. Future catalyst design will have to take this issue into consideration. In general, however, the reversible HAT at a stereogenic center is an efficient and economical way to convert racemic mixtures into enantiomerically pure compounds by the use of a single chiral photocatalyst.

ASSOCIATED CONTENT

Supporting Information

The Supporting Information is available free of charge at https://pubs.acs.org/doi/10.1021/jacs.2c11265.

Detailed experimental procedures; characterization data for new compounds; NMR titration experiments; deuteration experiments; coordinates for all computed structures; details on the computational methods and procedures; UV/Vis spectra of (−)-**2**; time-resolved UV/vis absorption spectroscopy data; NMR spectra for new compounds; and chiral HPLC traces including Figures S3.1−S8.3 and Tables S3.1−S6.3 (PDF)

NMR spectra of novel compounds (ZIP)

Optimized geometries of the molecules considered in the computational study (ZIP)

Molecular dynamics (MP4)

AUTHOR INFORMATION

Corresponding Authors

Christoph Bannwarth − *Institut für Physikalische Chemie, RWTH Aachen University, D-52074 Aachen, Germany;* orcid.org/0000-0003-3242-496X; Email: bannwarth@pc.rwth-aachen.de

Patrick Nuernberger − *Institut für Physikalische und Theoretische Chemie, Universität Regensburg, Regensburg D-93053, Germany;* orcid.org/0000-0002-4690-0229; Email: Patrick.Nuernberger@chemie.uni-regensburg.de

Thorsten Bach − *Department Chemie and Catalysis Research Center (CRC), School of Natural Sciences, Technische Universität München, D-85747 Garching, Germany;* orcid.org/0000-0002-1342-0202; Email: thorsten.bach@ch.tum.de

Authors

Roger Jan Kutta − *Institut für Physikalische und Theoretische Chemie, Universität Regensburg, Regensburg D-93053, Germany;* orcid.org/0000-0003-3368-9863

Johannes Großkopf − *Department Chemie and Catalysis Research Center (CRC), School of Natural Sciences, Technische Universität München, D-85747 Garching, Germany;* orcid.org/0000-0002-6540-3893

Nils van Staalduinen − *Institut für Physikalische Chemie, RWTH Aachen University, D-52074 Aachen, Germany*

Antonia Seitz − *Department Chemie and Catalysis Research Center (CRC), School of Natural Sciences, Technische Universität München, D-85747 Garching, Germany*

Philipp Pracht − *Institut für Physikalische Chemie, RWTH Aachen University, D-52074 Aachen, Germany; Yusuf Hamied Department of Chemistry, University of Cambridge, Cambridge CB2 1EW, United Kingdom*

Stefan Breitenlechner − *Department Chemie and Catalysis Research Center (CRC), School of Natural Sciences, Technische Universität München, D-85747 Garching, Germany;* orcid.org/0000-0001-5519-1922

Complete contact information is available at: https://pubs.acs.org/10.1021/jacs.2c11265

Author Contributions

[⊥]R.J.K. and J.G. contributed equally. The manuscript was written through contributions of all authors.

Notes

The authors declare no competing financial interest.

ACKNOWLEDGMENTS

Financial support by the *Deutsche Forschungsgemeinschaft* (Ba 1372/23 and TRR 325; projects A5, B2; 444632635) and the *Fonds der Chemischen Industrie* (Kekulé fellowship to JG) is gratefully acknowledged. C.B. acknowledges funding by the Federal Ministry of Education and Research (BMBF) and the Ministry of Culture and Science of the German State of North Rhine-Westphalia under the Excellence Strategy of the Federal Government and the *Länder*. We thank O. Ackermann (TU München) for his help with the HPLC analysis and Dr. Golo Storch (TU München) for inspiring, helpful discussions. Parts of the simulations were performed with computing resources granted by RWTH Aachen University under project rwth0721.

REFERENCES

(1) https://www.verifiedmarketresearch.com/product/chiral-chemicals-market/ (accessed Dec 16, 2022).

(2) Rouhi, A. M. Chiral Roundup. *Chem. Eng. News* **2002**, *80*, 43−50.

(3) (a) Akiyama, T.; Ojima, I. (Eds.) *Catalytic Asymmetric Synthesis*, 4th ed.; Weinheim, 2022. (b) Carreira, E. M.; Yamamoto, H. (Eds.) *Comprehensive Chirality*; Amsterdam, 2012. (c) Walsh, P. J.; Kozlowski, M. C.*Fundamentals of Asymmetric Catalysis*; Sausalito, 2009.

(4) Lorenz, H.; Seidel-Morgenstern, A. Processes to Separate Enantiomers. *Angew. Chem., Int. Ed.* **2014**, *53*, 1218−1250.

(5) Reviews: (a) Aranda, C.; Oksdath-Mansilla, G.; Bisogno, F. R.; de Gonzalo, G. Deracemisation Processes Employing Organocatalysis and Enzyme Catalysis. *Adv. Synth. Catal.* **2020**, *362*, 1233−1257. (b) Bhat, V.; Welin, E. R.; Guo, X.; Stoltz, B. M. Advances in Stereoconvergent Catalysis from 2005 to 2015: Transition-Metal-Mediated Stereoablative Reactions, Dynamic Kinetic Resolutions, and Dynamic Kinetic Asymmetric Transformations. *Chem. Rev.* **2017**, *117*, 4528−4561. (c) Palmans, A. R. A. Deracemisations under kinetic and thermodynamic control. *Mol. Syst. Des. Eng.* **2017**, *2*, 34−46. (d) Rachwalksi, M.; Vermue, N.; Rutjes, F. P. J. T. Recent advances in enzymatic and chemical deracemisation of racemic compounds. *Chem. Soc. Rev.* **2013**, *42*, 9268−9282. (e) Voss, C. V.; Gruber, C. C.; Kroutil, W. Deracemisation of Secondary Alcohols via Biocatalytic Stereoinversion. *Synlett* **2010**, 991−998.

(6) (a) Blackmond, D. G. "If Pigs Could Fly" Chemistry: A Tutorial on the Principle of Microscopic Reversibility. *Angew. Chem., Int. Ed.* **2009**, *48*, 2648−2654. (b) Kroutil, W.; Faber, K. Deracemization of compounds possessing a *sec*-alcohol or -amino group through a cyclic oxidation−reduction sequence: a kinetic treatment. *Tetrahedron: Asymmetry* **1998**, *9*, 2901−2913.

(7) (a) Hammond, G. S.; Cole, R. S. Asymmetric Induction during Energy Transfer. *J. Am. Chem. Soc.* **1965**, *87*, 3256−3257. (b) Drucker, C. S.; Toscano, V. G.; Weiss, R. G. General Method for the Determination of Steric Effects during Collisional Energy Transfer. Partial Photoresolution of Penta-2,3-diene. *J. Am. Chem. Soc.* **1973**, *95*, 6482−6484. (c) Ouannès, C.; Beugelmans, R.; Roussi, G. Asymmetric Induction during Transfer of Triplet Energy. *J. Am. Chem. Soc.* **1973**, *95*, 8472−8474.

(8) Reviews: (a) Yang, C.; Inoue, Y. An exciting tool for asymmetric synthesis. *Nature* **2018**, *564*, 197−199. (b) Shi, Q.; Ye, J. Deracemization Enabled by Visible-Light Photocatalysis. *Angew. Chem., Int. Ed.* **2020**, *59*, 4998−5001.

(9) Unselective photochemical reactions can also be combined with a kinetic resolution step. For a recent elegant example, see: Bierbaumer, S.; Schmermund, L.; List, A.; Winkler, C. K.; Glueck, S. M.; Kroutil, W. Synthesis of Enantiopure Sulfoxides by Concurrent Photocatalytic Oxidation and Biocatalytic Reduction. *Angew. Chem., Int. Ed.* **2022**, *61*, No. e202117103.

(10) Recent example: Zhang, Z.; Hu, X. Visible-Light-Driven Catalytic Deracemization of Secondary Alcohols. *Angew. Chem., Int. Ed.* **2021**, *60*, 22833−22838.

(11) (a) Hölzl-Hobmeier, A.; Bauer, A.; Silva, A. V.; Huber, S. M.; Bannwarth, C.; Bach, T. Catalytic deracemization of chiral allenes by sensitized excitation with visible light. *Nature* **2018**, *564*, 240−243. (b) Plaza, M.; Jandl, C.; Bach, T. Photochemical Deracemization of Allenes and Subsequent Chirality Transfer. *Angew. Chem., Int. Ed.* **2020**, *59*, 12785−12788.

(12) Bucher, G.; Mahajan, A. A.; Schmittel, M. The Photochemical C^2-C^6 Cyclization of Enyne-Allenes: Interception of the Fulvene Diradical with a Radical Clock Ring Opening. *J. Org. Chem.* **2009**, *74*, 5850−5860.

(13) Plaza, M.; Großkopf, J.; Breitenlechner, S.; Bannwarth, C.; Bach, T. Photochemical Deracemization of Primary Allene Amides by Triplet Energy Transfer: A Combined Synthetic and Theoretical Study. *J. Am. Chem. Soc.* **2021**, *143*, 11209−11217.

(14) Wimberger, L.; Kratz, T.; Bach, T. Photochemical Deracemization of Chiral Sulfoxides Catalyzed by a Hydrogen-Bonding Xanthone Sensitizer. *Synthesis* **2019**, *51*, 4417−4424.

(15) (a) Tröster, A.; Bauer, A.; Jandl, C.; Bach, T. Enantioselective Visible-Light-Mediated Formation of 3-Cyclopropylquinolones by Triplet-Sensitized Deracemization. *Angew. Chem., Int. Ed.* **2019**, *58*, 3538−3541. (b) Li, X.; Kutta, R. J.; Jandl, C.; Bauer, A.; Nuernberger, P.; Bach, T. Photochemically Induced Ring Opening of Spirocyclopropyl Oxindoles: Evidence for a Triplet 1,3-Diradical Intermediate and Deracemization by a Chiral Sensitizer. *Angew. Chem., Int. Ed.* **2020**, *59*, 21640−21647.

(16) Kratz, T.; Steinbach, P.; Breitenlechner, S.; Storch, G.; Bannwarth, C.; Bach, T. Photochemical Deracemization of Chiral Alkenes via Triplet Energy Transfer. *J. Am. Chem. Soc.* **2022**, *144*, 10133−10138.

(17) Shin, N. Y.; Ryss, J. M.; Zhang, X.; Miller, S. J.; Knowles, R. R. Light-driven deracemization enabled by excited-state electron transfer. *Science* **2019**, *366*, 364−369.

(18) Zhang, C.; Gao, A. Z.; Nie, X.; Ye, C.-X.; Ivlev, S. I.; Chen, S.; Meggers, E. Catalytic α-Deracemization of Ketones Enabled by Photoredox Deprotonation and Enantioselective Protonation. *J. Am. Chem. Soc.* **2021**, *143*, 13393−13400.

(19) Huang, M.; Zhang, L.; Pan, T.; Luo, S. Deracemization through photochemical *E*/*Z* isomerization of enamines. *Science* **2022**, *375*, 869−874.

(20) Review: Neveselý, T.; Wienhold, M.; Molloy, J. J.; Gilmour, R. Advances in the E → Z Isomerization of Alkenes Using Small Molecule Photocatalysts. *Chem. Rev.* **2022**, *122*, 2650−2694.

(21) Großkopf, J.; Plaza, M.; Seitz, A.; Breitenlechner, S.; Storch, G.; Bach, T. Photochemical Deracemization at sp^3-Hybridized Carbon Centers via a Reversible Hydrogen Atom Transfer. *J. Am. Chem. Soc.* **2021**, *143*, 21241−21245.

(22) For related work employing a reversible HAT for the epimerization of diastereoisomers, see: (a) Wang, Y.; Carder, H. M.; Wendlandt, A. E. Synthesis of rare sugar isomers through site-selective epimerization. *Nature* **2020**, *578*, 403−408. (b) Oswood, C. J.; MacMillan, D. W. C. Selective Isomerization via Transient Thermodynamic Control: Dynamic Epimerization of trans to cis Diols. *J. Am. Chem. Soc.* **2022**, *144*, 93−98. (c) Zhang, Y.-A.; Gu, X.; Wendlandt, A. E. A Change from Kinetic to Thermodynamic Control Enables trans-Selective Stereochemical Editing of Vicinal Diols. *J. Am. Chem. Soc.* **2022**, *144*, 599−605. (d) Kazerouni, A. M.; Brandes, D. S.; Davies, C. C.; Cotter, L. F.; Mayer, J. M.; Chen, S.; Ellman, J. A. Visible Light-Mediated, Highly Diastereoselective Epimerization of Lactams from the Most Accessible to the More Stable Stereoisomer. *ACS Catal.* **2022**, *12*, 7798−7803.

(23) For reviews on photochemical HAT, see: (a) Capaldo, L.; Ravelli, D.; Fagnoni, M. Direct Photocatalyzed Hydrogen Atom Transfer (HAT) for Aliphatic C−H Bonds Elaboration. *Chem. Rev.* **2022**, *122*, 1875−1924. (b) Cao, H.; Tang, X.; Tang, H.; Yuan, Y.; Wu, J. Photoinduced intermolecular hydrogen atom transfer reactions in organic synthesis. *Chem. Catal.* **2021**, *1*, 523−598. (c) Capaldo, L.; Quadri, L. L.; Ravelli, D. Photocatalytic hydrogen atom transfer: the philosopher's stone for late-stage functionalization? *Green Chem.* **2020**, *22*, 3376−3396. (d) Stateman, L. M.; Nakafuku, K. M.; Nagib, D. A. Remote C−H Functionalization via Selective Hydrogen Atom Transfer. *Synthesis* **2018**, *50*, 1569−1586.

(24) (a) Porter, G.; Suppan, P. Primary photochemical processes in aromatic molecules. Part 12. − Excited states of benzophenone derivatives. *Trans. Faraday Soc.* **1965**, *61*, 1664−1673. (b) Godfrey, T. S.; Hilpern, W.; Porter, G. Triplet-triplet absorption spectra of benzophenone and its derivatives. *Chem. Phys. Lett.* **1967**, *1*, 490−492. (c) Dormán, G.; Nakamura, H.; Pulsipher, A.; Prestwich, G. D. The Life of Pi Star: Exploring the Exciting and Forbidden Worlds of the Benzophenone Photophore. *Chem. Rev.* **2016**, *116*, 15284−15398.

(25) (a) Fielding, L. Determination of association constants (*Ka*) from solution NMR data. *Tetrahedron* **2000**, *56*, 6151−6170. (b) Thordarson, P. Determining association constants from titration experiments in supramolecular chemistry. *Chem. Soc. Rev.* **2011**, *40*,

https://doi.org/10.1021/jacs.2c11265
J. Am. Chem. Soc. 2023, 145, 2354−2363

1305−1323. (c) Bakowski, A.; Dressel, M.; Bauer, A.; Bach, T. Enantioselective radical cyclisation reactions of 4-substituted quinolones mediated by a chiral template. *Org. Biomol. Chem.* **2011**, *9*, 3516−3529.
(26) Simmons, E. M.; Hartwig, J. F. On the Interpretation of Deuterium Kinetic Isotope Effects in C-H Bond Functionalizations by Transition-Metal Complexes. *Angew. Chem., Int. Ed.* **2012**, *51*, 3066−3072.
(27) (a) Grimme, S.; Brandenburg, J. G.; Bannwarth, C.; Hansen, A. Consistent structures and Interactions by density functional theory with small atomic orbital basis sets. *J. Chem. Phys.* **2015**, *143*, No. 054107. (b) Neese, F. The ORCA program system. *WIREs Comput. Mol. Sci.* **2012**, *2*, 73−78. (c) Neese, F. Software update: the ORCA program system, version 4.0. *WIREs Comput. Mol. Sci.* **2018**, *8*, No. e1327.
(28) (a) Bannwarth, C.; Ehlert, S.; Grimme, S. GFN2-xTB: An Accurate and Broadly Parametrized Self-Consistent Tight-Binding Quantum Chemical Method with Multipole Electrostatics and Density-Dependent Dispersion Contributions. *J. Chem. Theory Comput.* **2019**, *15*, 1652−1671. (b) Asgeirsson, V.; Birgisson, B. O.; Bjornsson, R.; Becker, U.; Neese, F.; Riplinger, C.; Jonsson, H. Nudged Elastic Band Method for Molecular Reactions Using Energy − Weighted Springs Combined with Eigenvector Following. *J. Chem. Theory Comput.* **2021**, *17*, 4929−4945.
(29) (a) Grimme, S. Supramolecular Binding Thermodynamics by Dispersion-Corrected Density Functional Theory. *Chem. − Eur. J.* **2012**, *18*, 9955−9964. (b) Ehlert, S.; Stahn, M.; Spicher, S.; Grimme, S. Robust and Efficient Implicit Solvation Model for Fast Semiempirical Methods. *J. Chem. Theory Comput.* **2021**, *17*, 4250−4261. (c) Weigend, F.; Ahlrichs, R. Balanced basis sets of split valence, triple zeta valence and quadruple zeta valence quality for H to Rn: Design and assessment of accuracy. *Phys. Chem. Chem. Phys.* **2005**, *7*, 3297−3305. (d) Mardirossian, N.; Head-Gordon, M. *ω*B97X-V: A 10-parameter, range23 separated hybrid, generalized gradient approximation density functional with nonlocalcorrelation, designed by a survival-of-the-fittest strategy. *Phys. Chem. Chem. Phys.* **2014**, *16*, 9904−9924.
(30) Pracht, P.; Bannwarth, C. Fast Screening of Minimum Energy Crossing Points with Semiempirical Tight-Binding Methods. *J. Chem. Theory Comput.* **2022**, *18*, 6370−6385.
(31) (a) Bannwarth, C.; Yu, J. K.; Hohenstein, E. G.; Martinez, T. J. Hole-hole Tamm-Dancoff Approximated density functional theory: A highly efficient electronic structure method incorporating dynamic and static correlation. *J. Chem. Phys.* **2020**, *153*, No. 024110. (b) Yu, J. K.; Bannwarth, C.; Hohenstein, E. G.; Martinez, T. J. Ab Initio Nonadiabatic Molecular Dynamics with Hole-Hole Tamm-Dancoff Approximated Density Functional Theory. *J. Chem. Theory Comput.* **2020**, *16*, 5499−5511. (c) Seritan, S.; Bannwarth, C.; Fales, B. S.; Hohenstein, E. G.; Isborn, C. M.; Kokkila- Schumacher, S. I. L.; Li, X.; Liu, F.; Luehr, N.; Snyder, J. W., Jr.; Song, C.; Titov, A. V.; Umtsev, I. S.; Wang, L.-P.; Martinez, T. J. TeraChem: A graphical processing unit-accelerated electronic structure package for large-scale ab initio molecular dynamics. *WIREs Comput. Mol. Sci.* **2021**, *11*, No. e1494.
(32) For some key references on the characterization of enols, see: (a) Haspra, P.; Sutter, A.; Wirz, J. Acidity of Acetophenone Enol in Aqueous Solution. *Angew. Chem., Int. Ed.* **1979**, *18*, 617−619. (b) Capon, B.; Guo, B. Simple enols. 5. (Z)- and (E)-1-Hydroxy-1,3-butadiene. *J. Am. Chem. Soc.* **1988**, *110*, 5144−5147. (c) Chiang, Y.; Kresge, A. J. Enols and Other Reactive Species. *Science* **1991**, *253*, 395−400. (d) Mardyukov, A.; Eckhardt, A. K.; Schreiner, P. R. 1,1-Ethenediol: The Long Elusive Enol of Acetic Acid. *Angew. Chem., Int. Ed.* **2020**, *59*, 5577−5580.
(33) Bandyopadhyay, B.; Pandey, P.; Banerjee, P.; Samanta, A. K.; Chakraborty, T. CH···O Interaction Lowers Hydrogen Transfer Barrier to Keto−Enol Tautomerization of *β*-Cyclohexanedione: Combined Infrared Spectroscopic and Electronic Structure Calculation Study. *J. Phys. Chem. A* **2012**, *116*, 3836−3845.
(34) (a) McGarry, P. F.; Doubleday, C. E.; Wu, C.-H.; Staab, H. A.; Turro, N. J. UV—Vis Absorption Studies of Singlet to Triplet Intersystem Crossing Rates of Aromatic Ketones: Effects of Molecular Geometry. *J. Photochem. Photobiol., A* **1994**, *77*, 109−117. (b) Cai, X.; Sakamoto, M.; Fujitsuka, M.; Majima, T. Higher Triplet Excited States of Benzophenones and Bimolecular Triplet Energy Transfer Measured by Using Nanosecond−Picosecond Two-Color/Two-Laser Flash Photolysis. *Chem. − Eur. J.* **2005**, *11*, 6471−6477. (c) Aloïse, S.; Ruckebusch, C.; Blanchet, L.; Réhault, J.; Buntinx, G.; Huvenne, J.-P. The Benzophenone $S_1(n,\pi^*) \rightarrow T_1(n,\pi^*)$ States Intersystem Crossing Reinvestigated by Ultrafast Absorption Spectroscopy and Multivariate Curve Resolution. *J. Phys. Chem. A* **2008**, *112*, 224−231. (d) Marazzi, M.; Mai, S.; Roca-Sanjuán, D.; Delcey, M. G.; Lindh, R.; González, L.; Monari, A. Benzophenone Ultrafast Triplet Population: Revisiting the Kinetic Model by Surface-Hopping Dynamics. *J. Phys. Chem. Lett.* **2016**, *7*, 622−626. (e) Zvereva, E.; Segarra-Martí, J.; Marazzi, M.; Brazard, J.; Nenov, A.; Weingart, O.; Léonard, J.; Garavelli, M.; Rivalta, I.; Dumont, E.; Assfeld, X.; Haacke, S.; Monari, A. The Effect of Solvent Relaxation in the Ultrafast Time-Resolved Spectroscopy of Solvated Benzophenone. *Photochem. Photobiol. Sci.* **2018**, *17*, 323−331. (f) Venkatraman, R. K.; Kayal, S.; Barak, A.; Orr-Ewing, A. J.; Umapathy, S. Intermolecular Hydrogen Bonding Controlled Intersystem Crossing Rates of Benzophenone. *J. Phys. Chem. Lett.* **2018**, *9*, 1642−1648. (g) Venkatraman, R. K.; Orr-Ewing, A. J. Photochemistry of Benzophenone in Solution: A Tale of Two Different Solvent Environments. *J. Am. Chem. Soc.* **2019**, *141*, 15222−15229.
(35) (a) Tsubomura, H.; Yamamoto, N.; Tanaka, S. Transient Absorption Spectra of Benzophenone Studied by the Flash Excitation. *Chem. Phys. Lett.* **1967**, *1*, 309−310. (b) Buettner, A. V.; Dedinas, J. Photoreduction of Benzophenone in Benzene. II. Flash Photolysis Study of Primary Photochemical Reactions. *J. Phys. Chem.* **1971**, *75*, 187−191. (c) Topp, M. R. Activation-Controlled Hydrogen Abstraction by Benzophenone Triplet. *Chem. Phys. Lett.* **1975**, *32*, 144−149. (d) Brede, O.; Helmstreit, W.; Mehnert, R. Nanosekunden-Pulsradiolyse und Laserphotolyse von Benzophenon in Benzol und Cyclohexan. *Z. Phys. Chem.* **1975**, *256*, 505−512. (e) Hayashi, H. Direct Observation of the 1,4-Biradical of Benzophenone with Cis-3-Methyl-2-Pentene Excited by the Fourth Harmonic of a Nd:YAG Laser. *Bull. Chem. Soc. Jpn.* **1980**, *53*, 2201−2204. (f) Bensasson, R. V.; Gramain, J.-C. Benzophenone Triplet Properties in Acetonitrile and Water. Reduction by Lactams. *J. Chem. Soc., Faraday Trans. 1* **1980**, *76*, 1801−1810. (g) Encinas, M. V.; Scaiano, J. C. Reaction of Benzophenone Triplets with Allylic Hydrogens. Laser Flash Photolysis Study. *J. Am. Chem. Soc.* **1981**, *103*, 6393−6397. (h) Nagarajan, V.; Fessenden, R. W. Flash Photolysis of Transient Radicals. Benzophenone Ketyl Radical. *Chem. Phys. Lett.* **1984**, *112*, 207−211. (i) Ramseier, M.; Senn, P.; Wirz, J. Photohydration of Benzophenone in Aqueous Acid. *J. Phys. Chem. A* **2003**, *107*, 3305−3315. (j) Sakamoto, M.; Cai, X.; Hara, M.; Tojo, S.; Fujitsuka, M.; Majima, T. Transient Absorption Spectra and Lifetimes of Benzophenone Ketyl Radicals in the Excited State. *J. Phys. Chem. A* **2004**, *108*, 8147−8150.

https://doi.org/10.1021/jacs.2c11265
J. Am. Chem. Soc. 2023, 145, 2354−2363